九州大学学術情報リポジトリ
Kyushu University Institutional Repository

Study of Creep Resistance on the High Chrome Heat Resistant Steel for Component Steam Boiler Power Generation

Moch. Syaiful Anwar
Department of Metallurgical and Materials Engineering, Faculty of Engineering, Universitas Indonesia

Myrna Ariati Mochtar
Department of Metallurgical and Materials Engineering, Faculty of Engineering, Universitas Indonesia

Mabruri, Efendi
Research Center for Metallurgy, National Research and Innovation Agency, Kawasan Sains dan Teknologi (KST) B.J. Habibie

Eddy S. Siradj
Department of Metallurgical and Materials Engineering, Faculty of Engineering, Universitas Indonesia

https://doi.org/10.5109/7172310

出版情報：Evergreen. 11 (1), pp.470-480, 2024-03. Interdisciplinary Graduate School of Engineering Sciences, Kyushu University, Japan
バージョン：
権利関係：Creative Commons Attribution 4.0 International

KYUSHU UNIVERSITY

Study of Creep Resistance on the High Chrome Heat Resistant Steel for Component Steam Boiler Power Generation

Moch. Syaiful Anwar[1,2], Myrna Ariati Mochtar[1], Efendi Mabruri[2], Eddy S. Siradj[1,*]

[1]Department of Metallurgical and Materials Engineering, Faculty of Engineering, Universitas Indonesia, Kampus UI, Depok 16424, Indonesia

[2]Research Center for Metallurgy, National Research and Innovation Agency, Kawasan Sains dan Teknologi (KST) B.J. Habibie, Tangerang Selatan 15314, Indonesia

*Author to whom correspondence should be addressed:
E-mail: eddy.sumarno@ui.ac.id

(Received October 21, 2023; Revised January 29, 2024; Accepted March 05, 2024).

Abstract: The high chrome heat-resistant steel is commonly used as a part of an ultra-supercritical steam boiler and creep failures are usually observed after the part has been exposed to constant high boiler temperature operation. The heat-resistant steel 253 MA which contains high chrome of about 22 wt.% is usually found to be used for steam boiler pipe, so as it is interesting to investigate and evaluate the behavior of creep rupture of this steel and the relationship with microstructure and mechanical properties. The 253 MA heat-resistant steel material was cut and deformed using cold rolling to about 35% thickness reduction and heated at temperatures constant of 900, 1000, 1100 and 1200 ℃ for 0, 240, 420, 840, and 3600 seconds at each temperature under heating rate of 10 ℃/minutes and then quenched. Another high chrome heat-resistant steel 316L is also used as an investigated steel for validation of the austenite grain growth. The creep rupture test was carried out at a temperature of 700 ℃ and a stress of 150 MPa. The result of this study is evaluated as a modified model which describes the relationship of the Larson-Miller parameters between hardness and austenitic grain size, and it is found that the modified model seems to be in close agreement with another high chrome steel which has been reported in previous work.

Keywords: creep resistant; time of rupture; grain size; hardness; high chrome; heat resistant steel; empirical model

1. Introduction

Nowadays, power generation usually uses coal as a resource to fire the boiler. It can result in a negative effect of released emissions reaching 44% of global CO_2 emissions to the environment[1)]. To overcome this problem, high efficiency technology generates a low emission (HELE) need in steam power generation. There are several ways to achieve a HELE technology such as using Clean Coal Technology (CCT), fuel substitutions from low carbon to higher carbon, carbon capture and storage (CCS)[2)] and mostly using a heat-resistant steel containing several alloying elements which has high resistance to oxidation and creep, especially at a high temperature during boiler operation[3,4)]. There are several high temperature resistances of alloying such as ferritic high resistance stainless steel, austenitic stainless steel, and superalloy steel[3,5)]. Generally, heat resistance alloying steel has a high chromium content. However, steel containing very high chrome content tends to have brittle behavior due to deformation of α-phase at high temperature such as decrease of weldability and creep resistance. To maintain or increase both weldability and creep resistance, the element of nickel (Ni) is usually used as an alloying element added to the high chrome steel caused by generating a stable γ-phase or austenitic phase named austenitic stainless steel (ASS). There are many types of ASS, such as SS 316, 316L, and 253 MA which have high oxidation resistance also. For example, SS 316 when exposed in high temperature the oxide will be formed which is observed as chromium oxide (Cr_2O_3) on the surface of this steel[6)]. Furthermore, to avoid the formation of δ-ferrite, sometimes the element of copper is also used as alloying elements in addition to that steel[7–9)].

The chemical elements such as Mo, B, W, Nb, Ti, Hf, V, C, and N are added as alloying elements to steel a grade of heat-resistant steels when the steel is long exposed at high temperature and coating treatment to protect the steel

from severe high temperature[7,10]. The precipitate has been observed located in both grain boundaries and the matrix, whereas the role of the precipitate in this steel to retard the movement of dislocation[11]. The rare earth elements such as Rh, Ce, and Yt are also used as extra alloying elements to generate solid solutions. The creep rate of deformation become slowly due to the different size of solute and matrix atom, which retard the movement of dislocation, so it may influence the creep rupture time[12,13]. As reported if the creep deformation occurs caused by the grain boundaries sliding, the large grain size will have a high creep strength due to decreasing creep rate deformation[14].

Generally, creep deformation occurs in three stages: primary, secondary, and tertiary. In the first stage, the rate of creep deformation occurs faster than in the secondary stage, where in the second stage or secondary stage, the rate of creep deformation occurs sluggishly as increasing the creep time. At the third stage or tertiary stage, the creep deformation rate rapidly increases and reaches failure. The slope of secondary stage of the creep deformation is very important to predict the rate of activation energy, creep mechanism, creep strength, and rupture time[15].

The creep rate or strain rate model ($\dot{\varepsilon}_{f,min}$) and creep parameter are an important model in designing a high temperature material. Many empirical models of creep strain and parameters of creep have been developed and modified. However, the Norton model, which was the first empirical creep strain model developed in 1929[16] is usually used to determine creep strain rate, whereas the creep parameter of Larson-Miller is easier to evaluate creep lifetime or remaining life prediction than others creep parameter[17].

As has been reported previously[18,19], it is interesting to investigate the rate of creep deformation in steel grade of high chrome, because the rate of creep deformation of those steels is obtained by different results depending on the grade of the high chrome steel. Further investigation in this paper is to observe and evaluate creep deformation of the steel grade 253 MA containing 22 wt.% chrome elements. The objective of this investigation is to evaluate the relationship between the microstructure and creep rupture time and to evaluate the relationship between hardness and creep rupture time in terms of a modified model which can be used to predict the remaining life of this steel during operation in a boiler.

2. Materials and Methods

The steel grade containing high chrome 253 MA and 316L are used as an investigated material where the chemical composition of this material is measured by Optical Emission Spectroscopy (OES).

To evaluate the microstructure of these steels, the test steel is plastically deformed by using a cold rolling mill, thickness reduction of 35% and obtaining the final thickness of 2.3 mm. The test steel is heated in an induction furnace at temperatures of 900, 1000, and 1100 ℃ at heating time of 0, 240, 420, 840, and 3600 seconds for each temperature under a heating rate of 10 ℃/minutes and then quenched in water to form a different austenite grain size. In addition, the tested steel 253 MA is heated at a temperature of 1200 ℃.

The microstructure of the quenched steel is observed according to metallography procedure, from grinding using SiC paper grid 80 to 1500 and then polishing using alumina powder. To reveal the austenite grain boundaries, the polished steel is etched using aqua regia 4:1 around 4–30 s and then sprayed with water and alcohol and dryer. Austenitic grain boundaries are observed by using an optical microscope and the grain size is counted by intercept method according to ASTM E112 and application of image-J. The hardness of both the tested steel 253 MA and 316L were measured by using Vickers Hardness Tester using load of 0.3 N. The creep's plate specimen was prepared according to ASTM E8 by wire-cut electrical discharge machining (wire-cut EDM) which it can be machining complex geometries of subsize specimen[20]. The creep rupture test was performed at the temperature constant of 700 ℃ under the stress of 150 MPa by using ZwickRoell Creep Tester.

3. Result and Discussion

3.1 Chemical composition of 253 MA and 316L steel

The chemical composition of 253 MA and 316L steel-can be seen in Table 1, showing that the high chrome and nickel element was found in the 253 MA steel.

Table 1. The chemical composition of the investigated steel (%wt.)

Elements	Type	
	SS 253 MA	**SS 316L**
C	0.079	0.0042
Si	0.00089	0.7536
Mn	0.51	1.58
P	0.03	0.0038
S	<0.005	0.0009
Cr	22.06	17.36
Ni	10.86	9.35
Mo	0.08	2.14
N	0.384	-
Ce	0.03	-
La	0.014	-
Fe	Bal.	Bal.

3.2 Austenite grain growth kinetic of 253 MA and 316L steel

The microstructure of cold rolled steel 253 MA and 316L might be seen in Fig. 1 below, showing that the elongated austenite grain with twin deformation grain was observed. It has been reported previously[21–23] that a twin

deformation grain is formed in steel which has the unit crystal BCC, FCC and HCP. The twin deformation of austenite grain occurs due to the shearing force during cold plastic deformation and can be created by the image-mirror atom. It has been observed that the twin deformation austenite grain both 253 MA and 316L seems to be different grain size, whereas for cold rolled test steel, 253 MA is observed in bigger than for the 316L. The difference in the size of twin deformation grain is caused by differences in the prior austenite grain size of those tested steels, where the prior austenite grain of 253 MA is observed bigger compared with prior austenite grain of the 316L.

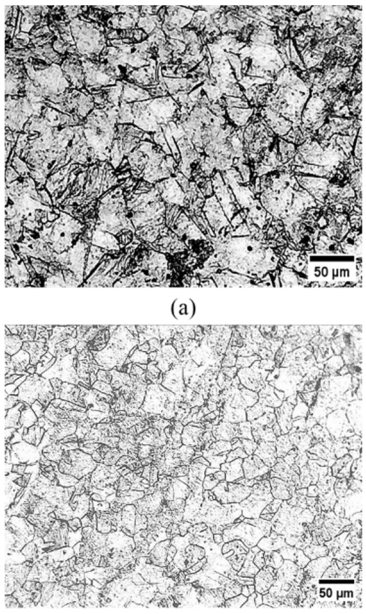

Fig. 1: Microstructure of heat resistance steel (a) 253 MA and (b) 316L after cold rolling

The deformation of twin austenite grains is triggered by critical stress during cold plastic deformation. The twin grain in steel having coarse prior austenite grain size seems easier to form due to low critical stress compared with the finer prior austenite grain, so as twining is observed much more than finer grain, as has been reported previously[24]. The austenite grain size of both tested steel 253 MA and 316L as shown in Fig. 2-4 increased as preheating temperature and holding time increased, and the annealing twin is also observed in the austenite grains.

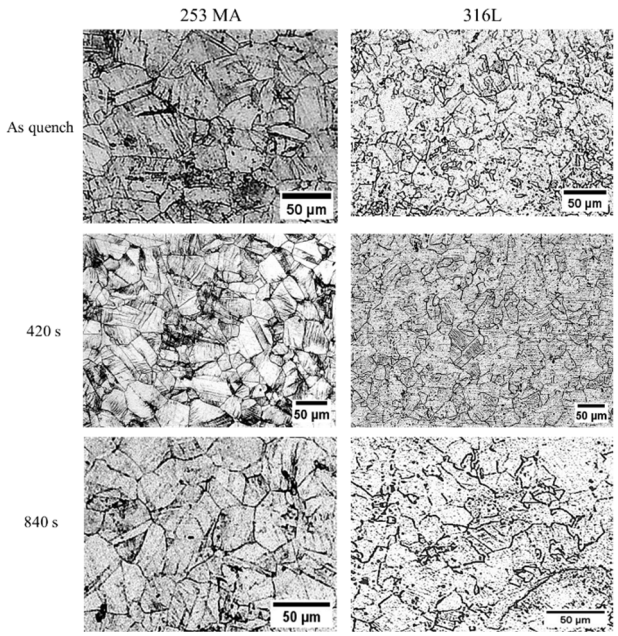

Fig. 2: Microstructure of heat resistance steel 253 MA and 316L after cold rolling as well as annealing 900 ℃ with variation of holding time

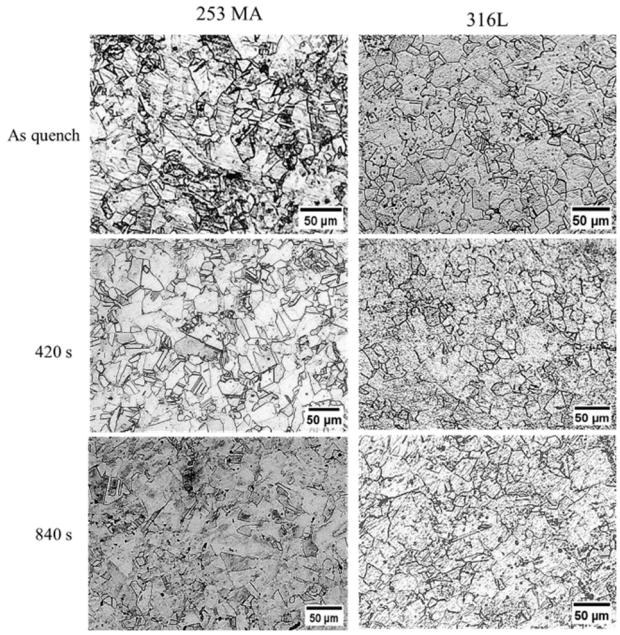

Fig. 3: Microstructure of heat resistance steel 253 MA and 316L after cold rolling as well as annealing 1000 ℃ with variation of holding time

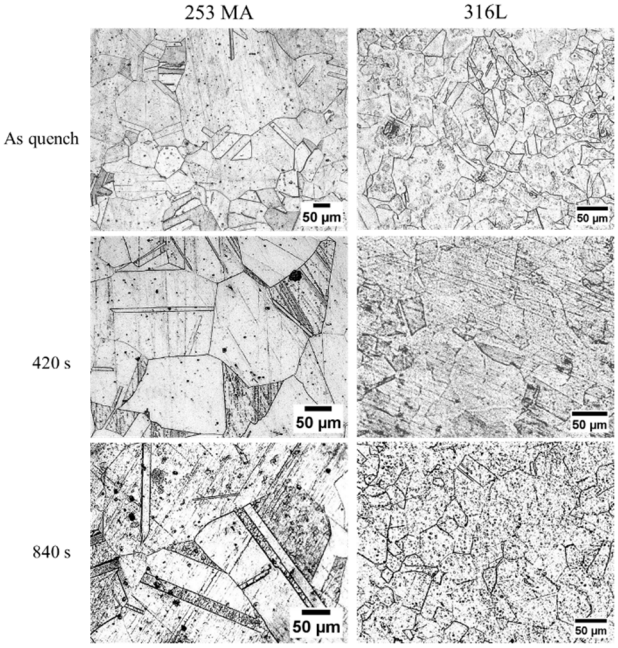

Fig. 4: Microstructure of heat resistance steel 253 MA and 316L after cold rolling as well as annealing 1100 ℃ with variation of holding time

These results seem to be in close agreement with those reported previously by Yue et al[25]. It has been mentioned that the recovery atom during austenite grain growth caused the formation of annealing twin grain in high chrome FCC steel which has a low stacking fault energy (SFE). The formation of twin grains due to atom recovery has been proposed by a growth accident model, where the model describes the atom move to the near lattice site and then to form twin grains[26]. The larger number and size of twins of 253 MA and 316L steel in Fig. 4(a-c) show that twins grow through the migration of twin boundaries.

To predict and evaluate the kinetic austenite grain growth in this steel, the tested steel was heated at the temperatures of 900, 1000, 1100 and 1200 ℃ at a holding time of 0, 240, 420 and 840 seconds for each temperature.

The empirical model that has been proposed by Yue et al[25] is adopted to evaluate the kinetic grain growth in the steel as can be rewritten in Eq. 1 below.

$$D^n - D_0^n = k_0 \cdot t^m \cdot EXP\left(-\frac{Q_g}{R \cdot T}\right) \quad (1)$$

The Eq. 1 then is modified in term of logarithmic equation in Eq. 2 below,

$$\ln(D^n - D_0^n) = \ln k_0 + m \cdot \ln t - \frac{Q_g}{2.3R} \cdot \frac{1}{T} \quad (2)$$

The austenitic grain growth result of both 253 MA and 316L steel can be seen in Fig. 5 below.

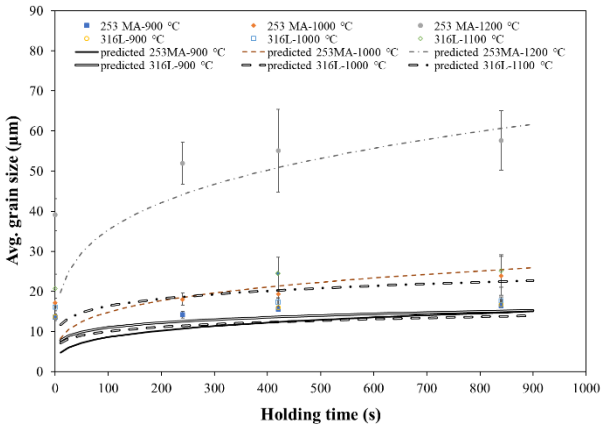

Fig. 5: Comparison of grain growth of 253 MA and 316L steel resulted of experiment and prediction

The relationship of $\ln(D^n - D_0^n)$ and ln t can be obtained from the slope of time exponent of m by assuming the value of the grain growth exponent of n is 0.5 – 5 according to Du et al[27] and Ji et al[28], and the activation energy of grain growth Q_{gg} can be predicted in the slope of $\ln(D^n - D_0^n)$ vs. 1/T. The values of k_0, m and n can be calculated by using the value of Q_{gg} as can be seen in Table 2 below.

Table 2. The value of Q_{gg}, k_0, m, and n on the 253 MA and 316L steel

Value		Steel type	
		SS 253 MA	SS 316L
k_0	900 ℃	1.3×10^{19}	4×10^{17}
	1000-1100 ℃		2×10^{16}
Q_{gg} (kJ/mol.K)		-376	-320
n		5.55	4.5
m		1.407	0.669

As can be seen in Table 2, the activation energy Q_{gg} of a high chrome steel type of 253 MA, the constant of k_0 and the grain growth exponent n as well as the time exponent of m were predicted much higher than a high chrome steel of 316L. It seems that some precipitated, is occurred in those steel are triggered by increasing of the value exponent grain growth of n which has been reported by Yue et al[25] and the value of constant k_0 is defending on both the chemical composition and processing condition has mentioned by Priadi et al[29]. The value of k_0 and n seem to have influenced the activation energy of grain growth (Q_{gg}) of these steels, and the high value of Q_{gg} can imply that the steel has a high stability of grain at a high temperature application. The activation energy depends on the manufacturing process also. For example, 316L steel in a wire shape[30] has higher activation energy than 316L in this experiment a which has a plate shape. According to Table 2, there are two models of grain growth for 253 MA and 316L steel that can be modified as shown in Eq. 3 and 4.

For 253 MA steel

$$D^{5.55} - D_0^{5.55} = 1.3x10^{19} \cdot t^{1.407} \cdot EXP\left(-\frac{376}{R \cdot T}\right) \quad (3)$$

For 316L steel

$$D^{4.5} - D_0^{4.5} = k_0 \cdot t^{0.669} \cdot EXP\left(-\frac{320}{R \cdot T}\right) \quad (4)$$

The predicted grain growth of those steels from Eq. 3 and 4 can be seen in Table 3 below.

Table 3. The predicted avg. grain size from grain growth model of Eq. 3 and 4

t (s)	Predicted avg. grain size, D (μm)					
	1173 K		1273 K		1373 K	1473 K
	253 MA	316L	253 MA	316L	316L	253 MA
10	4.79	7.83	8.27	7.13	11.63	19.72
25	6.04	8.97	10.43	8.17	13.33	24.88
50	7.21	9.94	12.44	9.06	14.78	29.66
75	7.99	10.56	13.78	9.62	15.69	32.87
100	8.59	11.02	14.83	10.04	16.38	35.36
125	9.09	11.39	15.69	10.38	16.93	37.41
150	9.52	11.70	16.43	10.67	17.40	39.18
175	9.90	11.98	17.09	10.91	17.80	40.75
200	10.24	12.22	17.67	11.13	18.16	42.15
225	10.55	12.43	18.21	11.33	18.48	43.43
250	10.84	12.63	18.70	11.51	18.77	44.60
275	11.10	12.81	19.16	11.67	19.04	45.69
300	11.35	12.97	19.59	11.82	19.29	46.71
325	11.58	13.13	19.99	11.96	19.52	47.67
350	11.80	13.28	20.37	12.10	19.73	48.57
375	12.01	13.41	20.73	12.22	19.94	49.43
400	12.21	13.54	21.07	12.34	20.13	50.25
425	12.40	13.66	21.39	12.45	20.31	51.02
450	12.58	13.78	21.71	12.56	20.48	51.77
475	12.75	13.89	22.01	12.66	20.65	52.48
500	12.92	14.00	22.29	12.76	20.81	53.17
525	13.08	14.10	22.57	12.85	20.96	53.83
550	13.23	14.20	22.84	12.94	21.11	54.47
575	13.38	14.29	23.10	13.02	21.25	55.09
600	13.53	14.38	23.35	13.11	21.38	55.68
625	13.67	14.47	23.59	13.19	21.51	56.26
650	13.81	14.55	23.83	13.26	21.64	56.83
675	13.94	14.64	24.06	13.34	21.76	57.37
700	14.07	14.72	24.28	13.41	21.88	57.90
725	14.19	14.79	24.50	13.48	21.99	58.42
750	14.32	14.87	24.71	13.55	22.10	58.93
775	14.44	14.94	24.91	13.61	22.21	59.42
800	14.55	15.01	25.12	13.68	22.31	59.90
825	14.67	15.08	25.31	13.74	22.42	60.37
850	14.78	15.15	25.51	13.80	22.52	60.83
875	14.89	15.21	25.69	13.86	22.61	61.27
900	14.99	15.28	25.88	13.92	22.71	61.71

As can be seen in Table 3, the grain growth of 253 MA steel during heating of 900 °C (1173 K) is slower than 316L steel. After heating of 1000–1200 °C (1273–1473 K), the grain growth of 253 MA steel is faster than 316L steel. It implies that the higher activation energy of grain growth of the 253 MA steel can affect the austenite grain to grow more rapidly when it is heated at above 1000 °C (1273 K).

The austenitic grain growth of these steels also can be confirmed by the change in grain boundary surface area per unit volume as seen in Eq. 5 below.

$$\text{Change in grain boundary surface area per unit volume } (\mu m^{-1}) = \frac{3}{D_f} - \frac{3}{D_i} \quad (5)$$

The change of grain boundary surface area per unit volume value of tested steel of 253 MA and 316L according to Eq. 5 has been presented in Fig. 6. These values did not increase significantly when the tested steels were heated between temperatures of 900 and 1000 °C, whereas the heating temperature of these steels above 1000 °C showed that the value change in grain boundary surface area per unit volume of 253 MA steel was higher than 316L steel. It implies that the high content of chromium in 253 MA steel was contributing to retard grain boundaries movement when it heated until 1000 °C.

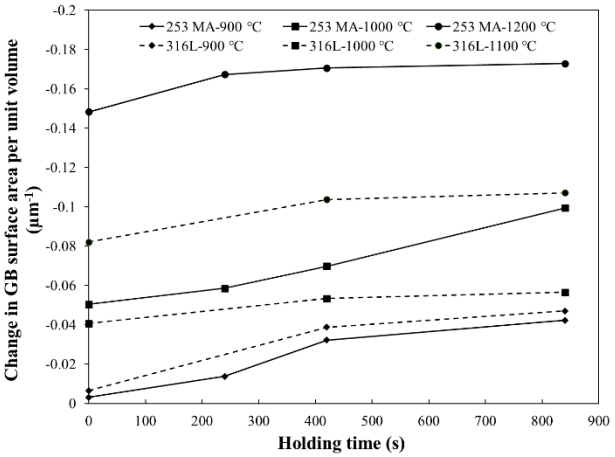

Fig. 6: The value of change in grain boundary surface area per unit volume on tested steel of 253 MA and 316L

3.3 Creep rupture behaviors

The behaviors of creep rupture on heat resistance steel only perform for high chrome steel type 253 MA steel, whereas high chrome steel type 316L is only used to investigate and evaluate the austenitic grain growth behavior. The tested steel 253 MA which varied the austenite grain size due to pre-heating at 900 °C and holding time of 0, 30, and 60 minutes were prepared as a creep test specimen with a gauge length of 25 mm and cross-section area of 13.8 mm². The steel is heated until it reaches a temperature creep of 700 °C and stress of 150 MPa was applied so that the uniaxial creep rupture test run until this steel occurred rupture. The experiment data of creep rupture test was plotted on the curve of creep strain with time of rupture as shown in Fig. 7. In this figure, the stage of primary, secondary, and tertiary creep has occurred in all grain size variance. Generally, the high grain size of the steel when applied at the high temperature of creep will cause a long rupture time for steel. For example, the steel with a grain size of 19.8 μm shows rupture time more rapidly than that grain size of 40.35 μm[31]. However, the rupture time of this steel, which has a grain size of 40.35 μm[31] occurred more slowly than that grain size of 50.99 μm[31] as displayed in Fig.7. It might be due to the appearance of a precipitate in the steel with a

grain size of 50.99 μm[31] that can initiate the micro-crack between precipitate and grain boundaries more rapidly than that the steel with a grain size of 40.35 μm[31]. The role precipitated by the crack propagation under creep deformation has been studied also in previous works[32–35].

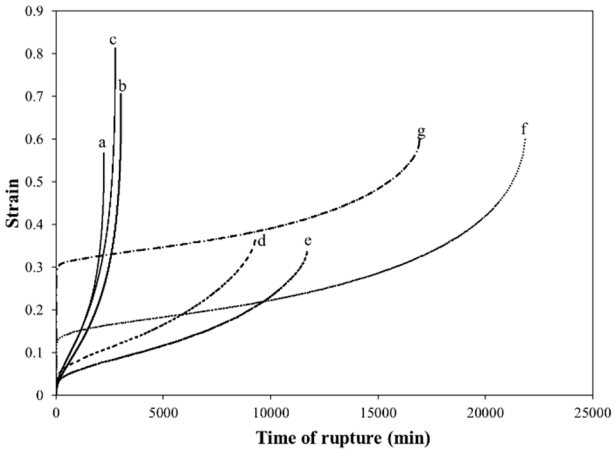

Fig. 7: Creep rupture of 253 MA steel on temperature of 700 °C and stress of 150 MPa with several grain size of (a) 19.8 μm, (b) 20.32 μm, (c) 22.87 μm, (d) 32.4 μm[31], (e) 34.88 μm[31], (f) 40.35 μm[31], and (g) 50.99 μm[31]

The value which are obtained on the creep rupture curve such as elastic strain (ε_e), fracture strain (ε_f), minimum creep rate ($\Delta\varepsilon/\Delta t$), and creep rupture time (t_r) were presented in Table 4. In this table, the high elastic strain of 0.306 mm/mm is found in steel with a grain size of 50.99 μm. The high fracture strain of 0.8132 mm/mm has been found in the steel with a grain size of 22.87 μm and a high minimum creep rate of 7.95×10^{-6} s^{-1} as well as been a high creep rupture time of 21846.14 min[31] was found in the steel which has a grain size of 40.35 μm.

Table 4. The value of creep rupture of 253 MA steel with grain size variation

D **(μm)**	ε_e	ε_f	$\Delta\varepsilon/\Delta t$ **(s^{-1})** $\times 10^{-6}$	t_r **(min)**	**Ref.**
19.80	0.242	0.5674	112.740	2227	This experiment
20.32	0.047	0.7058	116.431	3026	
22.87	0.025	0.8132	238.701	2756	
32.40	0.055	0.3670	22.1	9270	31)
34.88	0.039	0.3390	16.8	11684	
40.35	0.135	0.605	7.949	21846	
50.99	0.306	0.601	8.289	16924	

Fracture surface of creep rupture test 253 MA was also evaluated, where the creep rupture surface of 253 MA steel with grain size variation caused by the creep rupture test was observed using a SEM-EDS with magnification of 500X as shown in Fig. 8(a-g). In these figures, the brittle fracture shape and micro-cavities were clearly seen on the fracture surface in all of the grain size variations. This fracture can occur due to plastic deformation at high temperatures as a function of time. The precipitate in the grain boundaries can also trigger a micro-cavity or micro-crack, and it can propagate when constant stress and high temperatures apply until the steel ruptures. There are two types of fracture in these figures, intergranular and transgranular fracture. The intergranular fracture as shown in Fig. 8(a-e) occurred on the steel with grain size between 19.8 and 22.87 μm as well as a grain size of 34.88 μm[31] whereas the steel with grain size between 40.35 and 50.99 μm[31] suffered mix mode of fracture, intergranular and transgranular mixed fracture as shown in Fig. 8(f-g).

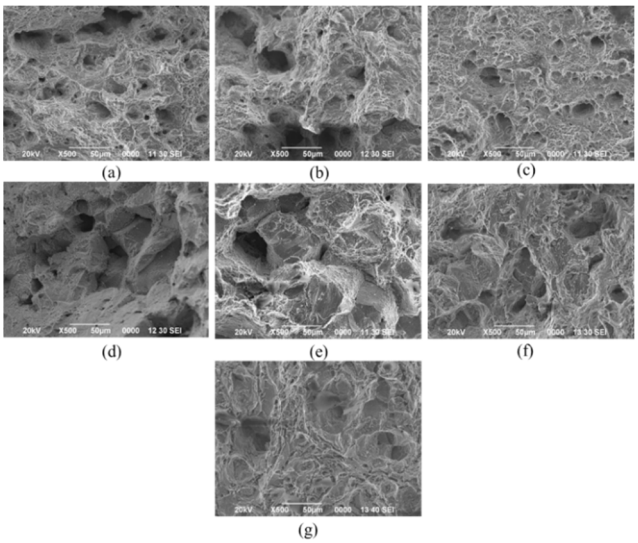

Fig. 8: Fractography of creep rupture 253 MA steel observed by using SEM with magnification of 500X at grain size of (a) 19.8 μm, (b) 20.32 μm, (c) 22.87 μm, compared with previous work (d) 32.4 μm[31], (e) 34.88 μm[31], (f) 40.35 μm[31], (g) 50.99 μm[31]

The mixed mode of fracture can be triggered by coalescence of a micro-cavity in the matrix grain and an intergranular crack in the grain boundary under creep rupture test[36]. The average creep cavity size in 253 MA steel is observed to be relatively small with a grain size of 19.8 to 22.87 μm compared with the grain size in the previous work[31]. The creep rupture of high chrome steel seems to be rapid due to course precipitate occurs in grain boundaries. It has been reported by Hu et al[32] that the size of creep cavity has a close relationship with stress concentrations on grain boundaries, having course precipitates which is triggered the creep rupture test much faster. According to the literature, the types of precipitate which are found in the heat resistance steel are $M_{23}C_6$, laves phase, Z-phase, and δ phase[32–35,37].

3.4 The relationship between austenitic grain and hardness with Larson-Miller parameter

The Larson-Miller parameter is usually used by researchers to predict creep rupture time and it can be rewritten in Eq. 6 below.

$$LMP = T(logt_r + C) \quad (6)$$

The relationship between the Larson-Miller parameter (LMP) and austenite grain size high chrome steel 253 MA is displayed in Fig. 9 below, as can be seen in this figure the LMP seems to be increased exponentially as austenite grain size increased.

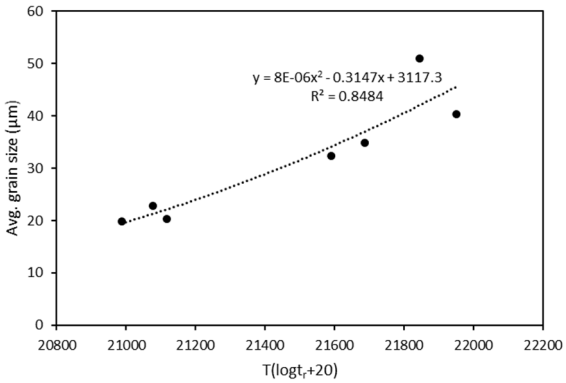

Fig. 9: Relationship between grain size and Larson Miller Parameter (LMP)

The slope relationship between LMP and grain size can be empirically modeled as shown in Eq. 7 below.

$$D = 8\,x\,10^{-6}(LMP)^2 - 0.3147(LMP) + 3117.3 \quad (7)$$

The empirical equation above (Eq. 7) can be modified as Eq. 8 below by using the relationship between LMP and the logarithmic austenite grain size as seen in Fig. 10.

$$\ln(D) = 9\,x\,10^{-4}(LMP) - 15.384 \quad (8)$$

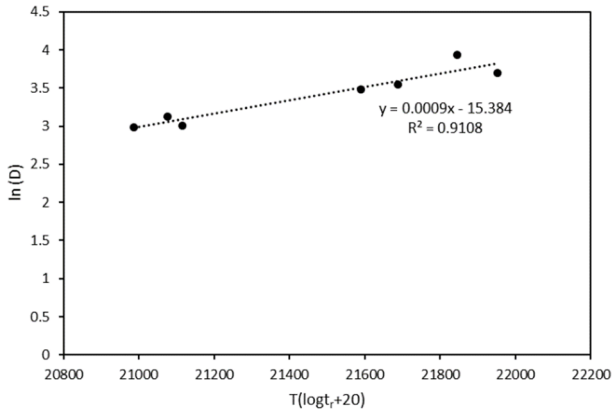

Fig. 10: Relationship ln (D) vs LMP

The modified empirical equation in Eq. 8 can be validated using another result which has been reported using several high chrome austenitic steels shown in Fig. 11.

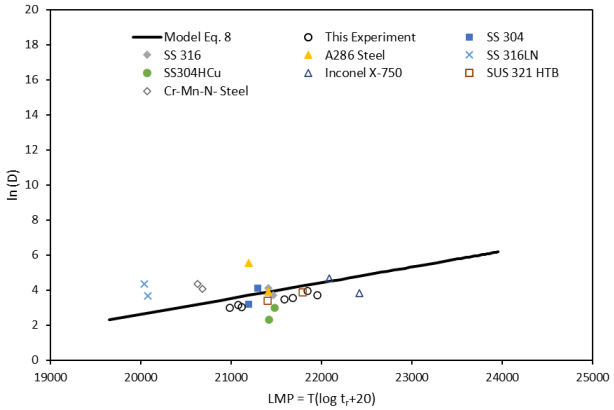

Fig. 11. Prediction of LMP using data experiment and model Eq. 8 and compared with previous result[38–45)]

From Fig. 11 above, it seems that a modified empirical model Eq. 8 to be closed in agreement with the result of other high chrome austenitic steel of SS 304, SS 316 and Inconel X-750 as well as SUS 312 HTB which has been reported from previous work.

On other hand, the relationship between the Larson-Miller parameter (LMP) and the hardness value of high chrome steel 253 MA is displayed in Fig. 12 below. In this figure, the initial hardness of steels is used to determine the relationship between hardness and LMP. This figure shows that LMP is increasing exponentially as the hardness decreases.

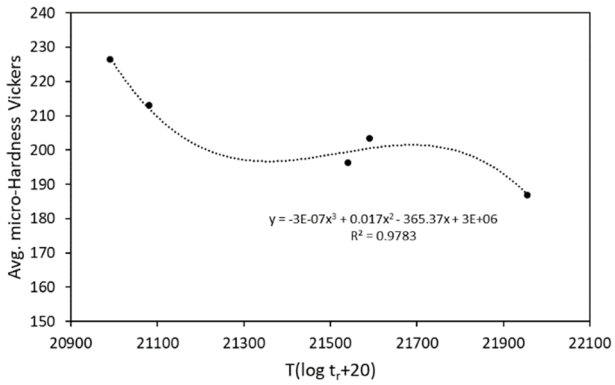

Fig. 12. Relationship between hardness and Larson Miller Parameter

The slope relationship between LMP and hardness can be empirically modeled as shown in Eq. 9 below.

$$HV = -3 \times 10^{-7}(LMP)^3 + 0.017(LMP)^2 - 365.37(LMP) + 3 \times 10^6 \quad (9)$$

The empirical equation above (Eq. 9) can be modified as Eq. 10 below by using the relationship between LMP and the logarithmic hardness as seen in Fig. 13.

$$\ln HV = 9.123 - 0.0002(LMP) \quad (10)$$

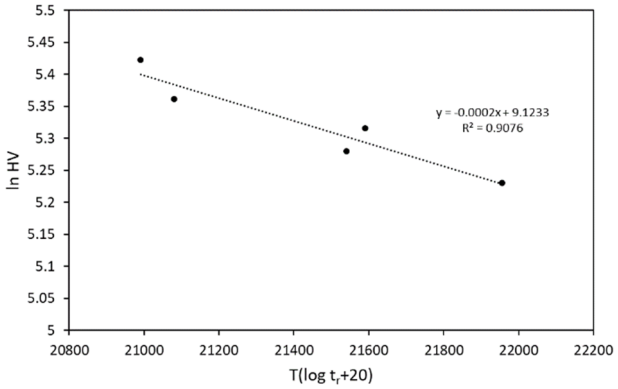

Fig. 13. Relationship between ln (HV) and LMP

The modified empirical equation in Eq. 10 can be validated using another result which has been reported using several low and high chrome austenitic steels shown in Fig. 14.

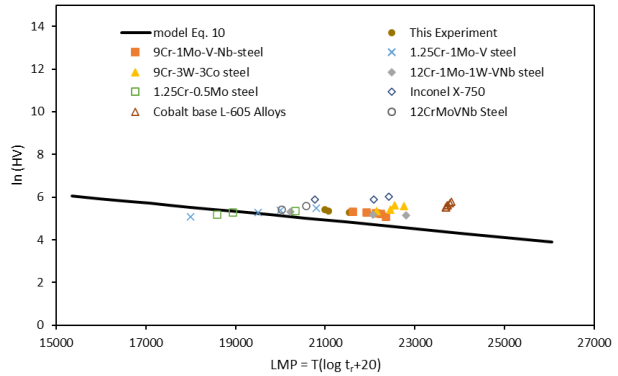

Fig. 14. Prediction of LMP using model Eq. 10 and compared with another result reported previously[43,46–52)]

From Fig. 14 above, it seems that a modified empirical model Eq. 10 to be closed in agreement with the result of another low chrome steel of 1.25Cr-1Mo-V, 1.25Cr-0.5Mo, 9Cr-1Mo-V-Nb, 9Cr-3W-3Co and high chrome steel 12Cr-1Mo-1W-VNb as well as 12CrMoVNb which has been reported by previously work.

4. Conclusions

The creep resistance of high chrome steel has been studied through the relationship between the microstructure and creep rupture time in terms of a modified model which can be used to predict the remaining life of this steel. The 253 MA steel, which has higher chrome elements as shown larger grain size and better creep resistance than 316L steel.

The grain growth of 253MA steel is faster than steel of 316L at a constant temperature, so the grain size of 253 MA steel is observed as larger than the grain size of 316L steel. The model kinetic of grain growth of those steel can be modified as below.

$D^{5.55} - D_0^{5.55} = 1.3x10^{19} \cdot t^{1.407} \cdot EXP\left(-\frac{376}{R \cdot T}\right)$ for 253 MA steel and

$D^{4.5} - D_0^{4.5} = k_0 \cdot t^{0.669} \cdot EXP\left(-\frac{320}{R \cdot T}\right)$ for 316L steel

The creep rupture time is in close relationship with the austenitic grain size of 253 MA steel, where the fine grain size is observed faster creep rupture time compared with the coarse grain size. The modified model of creep rupture time in terms of Larson-Miller Parameter can be described as the relationship with grain size can be modeled as

$$\ln(D) = 9\ x\ 10^{-4}(LMP) - 15.384$$

The hardness of 253 MA steel is influenced by the austenitic grain size, where the hardness of the steel decreases as the austenitic grain size increases. The modified model of creep rupture time in terms of Larson-Miller Parameter can be described as the relationship with hardness can be seen as

$$\ln HV = 9.123 - 2 \times 10^{-4}(LMP)$$

This modified model of creep rupture in terms of Larson-Miller Parameter would help evaluate remaining life for steel grade of high chrome for ultra-supercritical steam boiler application.

Acknowledgments

Moch. Syaiful Anwar and Eddy S. Siradj are equal authors. The authors would like to thank Seed Funding Professor Fakultas Teknik UI Tahun Anggaran 2022/2023 nomor: NKB-1937/UN2.F4.D/PPM.00.00/2022, and Joint Research with Research Center for Metallurgy-National Research and Innovation Agency (BRIN).

Nomenclature

D	average of grain size (μm)
D_0	initial average of grain size (μm)
t	holding time (s)
n	grain growth exponent
m	time exponent
Q_{gg}	activation energy of grain growth (kJ/mol.K)
k_0	pre-exponential term
R	general gas constant (8.31 J/K.mol)
T	temperature (K)
D_f	average of final grain size (μm)
D_i	average of initial grain size (μm)
t_r	creep rupture time (min, h)
LMP	larson miller parameter
C	constant
HV	Hardness vickers

Greek symbols

ε_e	elastic strain
ε_f	fracture strain
$\Delta\varepsilon/\Delta t$	minimum creep rate (s^{-1})

References

1) J. Santosa, Arief Heru Kuncoro, A. Dwijatmiko, Nurry Widya Hesty, and A. Darmawan, "The role of nuclear power plants in indonesia towards net zero emissions (nze) in 2060 with a multi regions approach," *Evergreen*, 10 (*3*) 1660–1673 (2023). doi:10.5109/7151715.
2) A. Wahid, D.R. Mustafida, and Y.A. Husnil, "Exergy analysis of coal-fired power plants in ultra supercritical technology versus integrated gasification combined cycle," *Evergreen*, 7 (*1*) 32–42 (2020). doi:10.5109/2740939.
3) A. Di Gianfrancesco, "The fossil fuel power plants technology," in: A. Di Gianfrancesco (Ed.), Materials for Ultra-Supercritical and Advanced Ultra-Supercritical Power Plants, Elsevier, 2017: pp. 1–49. doi:10.1016/B978-0-08-100552-1.00001-4.
4) H. Akamine, M. Mitsuhara, and M. Nishida, "Developments of coal-fired power plants: microscopy study of fe-ni based heat-resistant alloy for efficiency improvement," *Evergreen*, 3 (*2*) 45–53 (2016). doi:10.5109/1800871.
5) Y. Zhao, H.L. Liu, L.L. Wei, and L.Q. Chen, "An overview on the novel heat-resistant ferritic stainless steels," *Tungsten*, (2022). doi:10.1007/s42864-022-00171-4.
6) P.P.D.K. Wulan, J.A. Ningtyas, and M. Hasanah, "The effect of nickel coating on stainless steel 316 on growth of carbon nanotube from polypropylene waste," *Evergreen*, 6 (*1*) 98–102 (2019). doi:10.5109/2328411.
7) G. Golański, A. Zieliński, and H. Purzyńska, "Precipitation Processes in Creep-Resistant Austenitic Steels," in: Austenitic Stainless Steels - New Aspects, InTech, 2017. doi:10.5772/intechopen.70941.
8) M. Hättestrand, M. Schwind, and H.-O. Andrén, "Microanalysis of two creep resistant 9-12% chromium steels," *Materials Science and Engineering A*, 250 27–36 (1998).
9) Q. Wang, S. Chen, and L. Rong, "δ-ferrite formation and its effect on the mechanical properties of heavy-section aisi 316 stainless steel casting," *Metall Mater Trans A Phys Metall Mater Sci*, 51 (*6*) 2998–3008 (2020). doi:10.1007/s11661-020-05717-0.
10) S. kumar, Akash, A. K.C, and K. J, "Solid particle erosion performance of multi-layered carbide coatings (wc-sic-cr 3 c 2)," *EVERGREEN Joint Journal of Novel Carbon Resource Sciences & Green Asia Strategy*, 10(2) 813–819 (2023). doi.org/10.5109/6792833
11) R. Sandström, "Fundamental Models for the Creep of Metals," in: Creep, InTech, 2018. doi:10.5772/intechopen.70726.
12) R. Yang, X. Cai, L. Zheng, X. Hu, and D. Li, "Enhancement mechanism of cerium in 316ln austenitic stainless steel during creep at 700 °c," *Acta Metallurgica Sinica (English Letters)*, (2022). doi:10.1007/s40195-022-01467-7.
13) R. Yang, S. Ma, X. Cai, X. Hu, and D. Li, "Effect of ce on creep damage behavior of 316ln austenitic stainless steel at 700 °c," *Journal of Materials Research and Technology*, (2023). doi:10.1016/j.jmrt.2023.09.081.
14) K. Nie, W.P. Wu, X.L. Zhang, and S.M. Yang, "Molecular dynamics study on the grain size, temperature, and stress dependence of creep behavior in nanocrystalline nickel," *J Mater Sci*, 52 (*4*) 2180–2191 (2017). doi:10.1007/s10853-016-0506-3.
15) F. Sui, and R. Sandström, "Basic modelling of tertiary creep of copper," *J Mater Sci*, 53 (*9*) 6850–6863 (2018). doi:10.1007/s10853-017-1968-7.
16)F.H. Norton, "The creep of steel at high temperatures," McGraw-Hill book company, inc, New York, 1929. https://archive.org/details/creepofsteelathi00nort/page/n1/mode/2up (accessed January 27, 2024).
17) Z. Abdallah, V. Gray, M. Whittaker, and K. Perkins, "A critical analysis of the conventionally employed creep lifing methods," *Materials*, 7 (*5*) 3371–3398 (2014). doi:10.3390/ma7053371.
18) K.C. Sahoo, S. Goyal, P. Parameswaran, S. Ravi, and K. Laha, "Assessment of creep deformation, damage, and rupture life of 304hcu austenitic stainless steel under multiaxial state of stress," *Metall Mater Trans A Phys Metall Mater Sci*, 49 (*3*) 881–898 (2018). doi:10.1007/s11661-017-4459-1.
19) N. Kumar, and S.D. Yadav, "Creep curve modelling of austenitic steel 316ln," *IOP Conf Ser Mater Sci Eng*, 1248 (*1*) 012022 (2022). doi:10.1088/1757-899x/1248/1/012022.
20) A. Supawi, S. Ahmad, N.F. Mohd Joharudin, and F. Karim, "Surface integrity of rbd palm oil as a bio degradable oil based dielectric fluid on sustainable electrical discharge machining (edm) of aisi d2 steel," *Evergreen*, 9 (*1*) 41–48 (2022). doi:10.5109/4774215.
21) Z.H. Aitken, and Y.W. Zhang, "Revealing the deformation twinning nucleation mechanism of bcc heas," *MRS Commun*, 9 (*1*) 406–412 (2019). doi:10.1557/mrc.2019.16.
22) L. Wang, P. Guan, J. Teng, P. Liu, D. Chen, W. Xie, D. Kong, S. Zhang, T. Zhu, Z. Zhang, E. Ma, M. Chen, and X. Han, "New twinning route in face-centered cubic nanocrystalline metals," *Nat Commun*, 8 (*1*) (2017). doi:10.1038/s41467-017-02393-4.
23) C.Y. Hung, Y. Bai, T. Shimokawa, N. Tsuji, and M. Murayama, "A correlation between grain boundary character and deformation twin nucleation mechanism in coarse-grained high-mn austenitic

steel," *Sci Rep*, 11 (*1*) (2021). doi:10.1038/s41598-021-87811-w.
24) I.A. Ovid'ko, R.Z. Valiev, Y.T. Zhu, A. Ilya, and K. Ovid', "Review on superior strength and enhanced ductility of metallic nanomaterials," *Prog Mater Sci*, 94 462–540 (2018).
25) C. Yue, L. Zhang, S. Liao, and H. Gao, "Kinetic analysis of the austenite grain growth in gcr15 steel," *J Mater Eng Perform*, 19 (*1*) 112–115 (2010). doi:10.1007/s11665-009-9413-y.
26) Y. Jin, B. Lin, M. Bernacki, G.S. Rohrer, A.D. Rollett, and N. Bozzolo, "Annealing twin development during recrystallization and grain growth in pure nickel," *Materials Science and Engineering A*, 597 295–303 (2014). doi:10.1016/j.msea.2014.01.018.
27) S. Du, Y. Li, and Y. Zheng, "Kinetics of austenite grain growth during heating and its influence on hot deformation of lz50 steel," *J Mater Eng Perform*, 25 (*7*) 2661–2669 (2016). doi:10.1007/s11665-016-2162-9.
28) G. Ji, X. hua Gao, Z. guang Liu, and K. Zhang, "In situ observation and modeling of austenite grain growth in a nb–ti-bearing high carbon steel," *Journal of Iron and Steel Research International*, 26 (*3*) 292–300 (2019). doi:10.1007/s42243-018-0083-6.
29) D. Priadi, R.A.M. Napitupulu, and E.S. Siradj, "Austenite grain growth calculation of 0.028% nb steel," *Journal of Mining and Metallurgy, Section B: Metallurgy*, 47 (*2*) 199–209 (2011). doi:10.2298/JMMB100901001P.
30) B.E. Kashyap, and K. Tangri, "Grain growth behaviour of type 316l stainless steel," *Materials Science and Engineering A,* 149 L 13-L 16 (1992).
31) M.S. Anwar, R.R. Widjaya, L.B.A. Prasetya, A.A. Arfi, E. Mabruri, and E.S. Siradj, "Effect of grain size on mechanical and creep rupture properties of 253 ma austenitic stainless steel," *Metals (Basel)*, 12 (*5*) (2022). doi:10.3390/met12050820.
32) Z.F. Hu, and Z. Zhang, "Investigation the effect of precipitating characteristics on the creep behavior of hr3c austenitic steel at 650 ℃," *Materials Science and Engineering A*, 742 451–463 (2019). doi:10.1016/j.msea.2018.10.124.
33) L. Cui, H. Gao, H. Li, Y. Liu, D. Wang, and W. Ding, "Effect of precipitate evolution on creep damage of reduced activation ferritic/martensitic steel friction stir welded joint," *J Alloys Compd*, 808 (2019). doi:10.1016/j.jallcom.2019.151738.
34) Y. Yamamoto, M.P. Brady, Q.Q. Ren, J.D. Poplawsky, D.T. Hoelzer, and M.J. Lance, "Creep behavior and phase equilibria in model precipitate strengthened alumina-forming austenitic alloys," *JOM*, (2022). doi:10.1007/s11837-022-05203-5.
35) H. Han, J. Shen, and J. Xie, "Effects of precipitates evolution on low stress creep properties in p92 heat-resistant steel," *Sci Rep*, 8 (*1*) (2018). doi:10.1038/s41598-018-33814-z.
36) M. Tanaka, J. Taguchi, and R. Kato, "Effects of microstructures on the creep-rupture properties and fracture mechanisms in austenitic heat-resistant steels," *Materials Science and Engineering A*, 410–411 79–84 (2005). doi:10.1016/j.msea.2005.08.007.
37) S. Zhang, L. Wang, X. Lin, H. Yang, M. Li, L. Lei, and W. Huang, "Precipitation behavior of δ phase and its effect on stress rupture properties of selective laser-melted inconel 718 superalloy," *Compos B Eng*, 224 (2021). doi:10.1016/j.compositesb.2021.109202.
38) M. Tanaka, Y. Ito, R. Kato, and A. Kayama, "Grain size dependence of creep-rupture properties and fracture mechanism in austenitic sus304 steel at 973 k," *J Mater Sci Lett*, 19 899–902 (2000).
39) S.L. Mannan, and P. Rodriguez, "Effect of grain size on creep rate in type 316 stainless steel at 873 and 973 k," *Metal Science*, 17 63–69 (1983).
40) S.M. Zhu, F.G. Wang, and S.J. Zhu, "Grain size dependence of creep crack growth in ni-cr austenitic steels," *Mater Trans*, 34 450–454 (1993).
41) Y.S. Lee, W. Kim, Y. Lee, and W.S. Ryu, "Effect of grain size on creep properties of type 316ln stainless steel," *Metals and Materials International*, 7 (*2*) 107–114 (2001).
42) A. Jeyaraj, V.D. Vijayanand, V. Ganesan, D. Ravindran, G.V.P. Reddy, S. Sankaran, and S.L. Mannan, "Grain size effect on creep properties of 304hcu ss and modelling of creep curves using modified theta projection approach," *Transactions of the Indian National Academy of Engineering*, 7 (*2*) 635–643 (2022). doi:10.1007/s41403-021-00301-3.
43) M. Tanaka, and R. Kato, "The effect of heat treatments on the creep-rupture properties of a wrought ni-cr heat-resistant alloy at 973 k," *J Mater Sci*, 45 (*15*) 4029–4035 (2010). doi:10.1007/s10853-010-4481-9.
44) F. Abe, "Heat-to-heat variation in creep life and fundamental creep rupture strength of 18cr-8ni, 18cr-12ni-mo, 18cr-10ni-ti, and 18cr-12ni-nb stainless steels," *Metall Mater Trans A Phys Metall Mater Sci*, 47 (*9*) 4437–4454 (2016). doi:10.1007/s11661-016-3587-3.
45) V.V.P. Kutumbarao, and P.R. Rao, "Effect of grain size on the creep and creep rupture behaviour of a cr-mn-n austenitic stainless steel," *Scripta Metallurgica*, 7 1003–1010 (1973).
46) F. Masuyama, "Hardness model for creep-life assessment of high-strength martensitic steels," *Materials Science and Engineering A*, 510–511 (*C*) 154–157 (2009). doi:10.1016/j.msea.2008.04.133.
47) K. Fujiyama, K. Kimura, and M. Yamada, "Evaluation through of creep properties hardness of measurement degraded cr-mo-v turbine cast steels and its application to life assessment the virgin material test blocks and turbine cast components for investigation were fabricated frorn," *ISIJ International*, 30 (*lO*) 869–874 (1990).

48) E. El-Kashif, K. Asakura, and K. Shibata, "Effects of nitrogen in 9cr-3w-3co ferritic heat resistant steels containing boron," *ISIJ International*, 42 (*12 SPEC.*) 1468–1476 (2002). doi:10.2355/isijinternational.42.1468.
49) F. Abe, "Progress in creep-resistant steels for high efficiency coal-fired power plants," *Journal of Pressure Vessel Technology, Transactions of the ASME*, 138 (*4*) (2016). doi:10.1115/1.4032372.
50) M. Demikrol, "On the creep strength-rupture ductility behaviour of 1.25cr-0.5mo low alloy steel," *Turkish Journal of Engineering and Environmental Sciences*, 23 389–401 (1999).
51) M. Tanaka, and H. Iizuka, "Effects of high-temperature ageing on the creep-rupture properties of cobalt-base l-605 alloys," *J Mater Sci*, 25 5199–5206 (1990).
52) Y.S. Lee, and J. Yu, "Effect of matrix hardness on the creep properties of a 12crmovnb steel," *Metallurgical and Materials Transactions A*, 30A 2331–2339 (1999).